RESEARCH ARTICLE

ADVANCED MATERIALS
www.advmat.de

Polarization Saturation in Multilayered Interfacial Ferroelectrics

*Wei Cao, Swarup Deb, Maayan Vizner Stern, Noam Raab, Michael Urbakh, Oded Hod, Leeor Kronik, and Moshe Ben Shalom**

Van der Waals polytypes of broken inversion and mirror symmetries have been recently shown to exhibit switchable electric polarization even at the ultimate two-layer thin limit. Their out-of-plane polarization has been found to accumulate in a ladder-like fashion with each successive layer, offering 2D building blocks for the bottom-up construction of 3D ferroelectrics. Here, it is demonstrated experimentally that beyond a critical stack thickness, the accumulated polarization in rhombohedral polytypes of molybdenum disulfide saturates. The underlying saturation mechanism, deciphered via density functional theory and self-consistent Poisson–Schrödinger calculations, point to a purely electronic redistribution involving: 1. Polarization-induced bandgap closure that allows for cross-stack charge transfer and the emergence of free surface charge; 2. Reduction of the polarization saturation value, as well as the critical thickness at which it is obtained, by the presence of free carriers. The resilience of polar layered structures to atomic surface reconstruction, which is essentially unavoidable in polar 3D crystals, potentially allows for the design of new devices with mobile surface charges. The findings, which are of general nature, should be accounted for when designing switching and/or conductive devices based on ferroelectric layered materials.

1. Introduction

Symmetry manipulation by stacking order control in 2D crystals has been identified as a route for accessing various ferroelectric phases in 2D material stacks.[1–11] For example, broken inversion and mirror symmetries in rhombohedral (r) stacks of van der Waals (vdW) materials made of binary compounds, e.g., boron nitride (BN) and various transition metal dichalcogenides (TMDs), lead to spontaneous interlayer charge transfer and the emergence of interface-confined electric fields. More recently, the same effect, albeit with a smaller magnitude, has been observed in pure graphene stacks.[12–14] The interfacial nature of the emerging polarization fields makes the effect robust against external depolarization factors, such as surface effects and doping.[7] Such materials, therefore, may serve as 2D building blocks for the bottom-up construction of 3D ferroelectrics.

For few-layered stacks, the interfacial polarization has been found to accumulate with each successive layer by distinct and evenly spaced ladder-like electric potential steps.[7] Clearly, such accumulation of polarization cannot proceed indefinitely, as for a thick enough stack the potential drop across the sample will induce cross-stack charge transfer that would inhibit further increase of the polarization.[15] Such saturation of the polarization is a general phenomenon that is by no means limited to stacked materials. However, following it experimentally in 3D polar semiconductors, e.g., GaN or AlN, or in oxide ferroelectrics such as $LaAlO_3$, is greatly complicated by the presence of additional effects, e.g., ion mixing, surface and interface reconstruction, the possible presence of contaminants, and the formation of surface defects.[16–22] On the contrary, stacked materials comprise of chemically stable individual sheets and, therefore, offer a unique opportunity for the direct observation of this underlying physical effect. Moreover, by avoiding surface ionic mixing and structural reorganization, the accumulated potential can, in principle, generate mobile surface carriers, which were so far limited to epitaxial interfaces of polar semiconductors.

In this study, we follow the evolution of polarization with stack thickness in MoS_2 using Kelvin-probe force microscopy (KPFM) measurements and directly observe its saturation. The results are explained via first principles calculations based on density

---

W. Cao[+], M. Urbakh, O. Hod
Department of Physical Chemistry
School of Chemistry
The Raymond and Beverly Sackler Faculty of Exact Sciences and The Sackler Center for Computational Molecular and Materials Science
Tel Aviv University
Tel Aviv 6997801, Israel

S. Deb, M. V. Stern, N. Raab, M. B. Shalom
School of Physics and Astronomy
Tel Aviv University
Tel Aviv 6997801, Israel
E-mail: moshebs@tauex.tau.ac.il

L. Kronik
Department of Molecular Chemistry and Materials Science
Weizmann Institute of Science
Rehovoth 7610001, Israel

The ORCID identification number(s) for the author(s) of this article can be found under https://doi.org/10.1002/adma.202400750

[+]Present address: State Key Laboratory of Materials-Oriented Chemical Engineering, Nanjing Tech University, Nanjing, Jiangsu 210009, China

DOI: 10.1002/adma.202400750

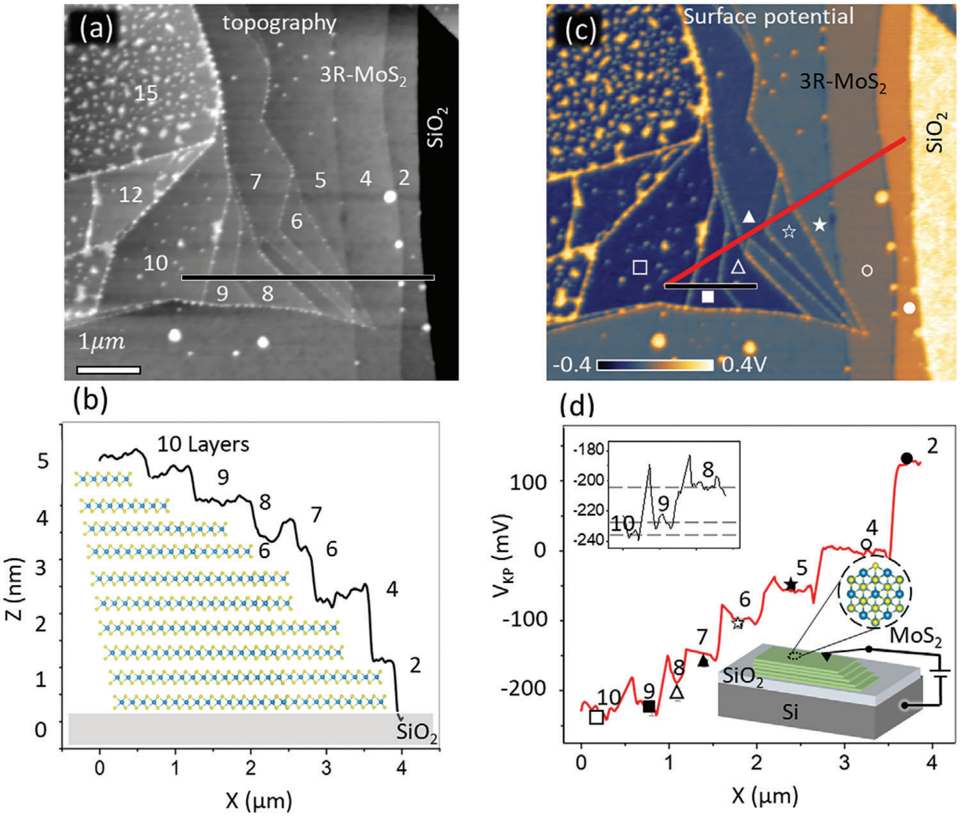

Figure 1. Surface topography and potential of polar multilayer MoS$_2$. a) AFM topography map of an MoS$_2$ flake exfoliated onto a SiO$_2$ surface. Numbers in white indicate number of MoS$_2$ layers. b) Topographic cross-section cut along the black line marked in panel (a). The number of layers in each step is stated, and the stacking sequence is sketched. c) Surface potential map of the flake shown in panel a, measured by an AFM tip operated at the Kelvin probe mode. d) Cross-sectional cuts of the surface potential map measured along the red (main panel) and black (inset) lines in panel (c), with various symbols corresponding to planes designated by the same symbol in panel (c). A sketch of the experimental setup is also shown.

functional theory (DFT). Specifically, the calculations show that the saturated polarization value depends strongly on the presence of free carriers in the 2D stack, which must be accounted for in order to obtain quantitative agreement between theory and experiment.

2. Results and Discussion

To probe the evolution of the spontaneous polarization with the number of layers, we measured the electric surface potential of r-MoS$_2$ flakes exfoliated onto a SiO$_2$/Si substrate (see Sections S1.1 and S1.2, Supporting Information). An atomic force microscope (AFM) operated at topography mode was used to measure the crystal thickness and deduce the number of layers, N (see **Figure** 1a,b). The microscope was then used in KPFM mode to scan the same region and obtain a surface potential, V_{KP}, map (see Figure 1c,d, with an additional example given in Section S1.3, Supporting Information). We focus on flakes containing regions of different thickness, ranging from 2 to 15 layers, all exhibiting co-aligned interfacial polarizations. The crystalline stacking configuration and the measurement setup are illustrated in Figure 1b,d, respectively. Figure 1d presents a surface potential line cut that spans stack thicknesses of 2–10 layers. Up to $N = 7$, the potential profile exhibits constant V_{KP} steps of $\Delta V_{\mathrm{KP}} = 56$ mV per additional layer, indicating a cumulative interfacial effect.[7] Notably, above $N = 8$ layers the surface potential steps decrease in size, resulting in an approach towards saturation, as discussed below. The potential jumps appearing near the physical step positions are attributed to surface contamination near step edges, which are manifested in the topography map (Figure 1a) as bright spots. The surface contamination density increases with stack thickness, possibly due to the increased surface potential (see Figure 1c). A similar trend has been observed for several other flakes (see results for three more devices in Section S1.3, Supporting Information). To eliminate the effect of surface adsorbates on the reported surface potential, we averaged V_{KP} over clean step surface regions, marked by various symbols in Figure 1c, where the potential map exhibits a uniform value, ruling out lateral charge distribution effects. The same data are presented also in **Figure** 2a (Device 1), where for convenience the shifted absolute value, $|V_{\mathrm{KP}}(N) - V_{\mathrm{KP}}(1)|$, is plotted, where $V_{\mathrm{KP}}(N)$ is the value obtained over a region of N layers and the potential above a single layer, $V_{\mathrm{KP}}(1)$, is extracted as described in Section S1.4 (Supporting Information). The potential saturation is found to occur at a value of 0.42 V. Similar measurements of three other devices are further shown (Devices 2, 3, and 4). They exhibit constant potential steps of $\Delta V = 78$, 63, and 73 meV/layer up to $N \approx 8$, with saturation at 0.57, 0.4, and 0.43 V, respectively. Devices

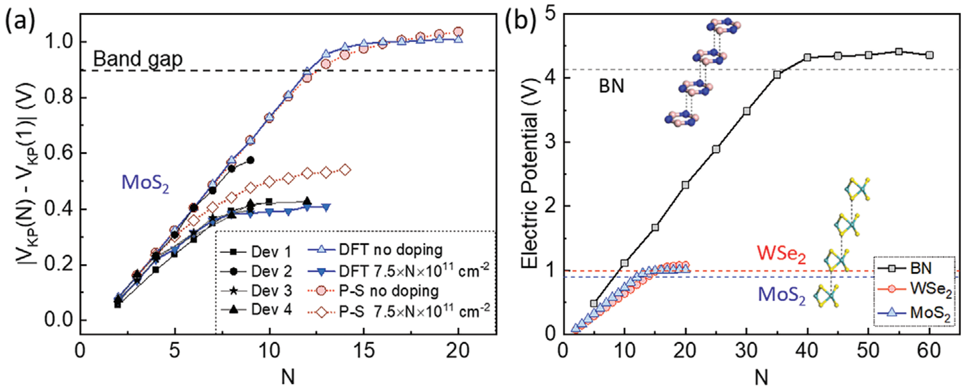

Figure 2. Surface potential saturation with stack thickness. a) Black symbols: measured averaged surface potential changes, $|V_{KP}(N) - V_{KP}(1)|$, as a function of the number of layers, N, for four representative *r*-MoS$_2$ flakes, each containing regions of various thicknesses (Device 1 is the same as in Figure 1). Blue upright and downward facing triangles: DFT calculations of the total potential difference across separate *r*-crystals with co-polarized interfaces, under zero doping and under an electronic doping level of 7.5×10^{11} e cm^{-2} per layer, respectively. The DFT-calculated bulk MoS$_2$ bandgap (an underestimate of the experimental one, see text) is given by a dashed horizontal line. Red circle and rhombus symbols: surface potential values obtained via the Poisson–Schrödinger model for the same structures with no doping and under an electron doping of 7.5×10^{11} e cm^{-2} per layer, respectively. b) DFT polarization calculations comparing the saturation curves of structurally relaxed *r*-MoS$_2$, *r*-WSe$_2$, and *r*-BN multilayers.

3 and 4 also show stacking faults with domains of anti-aligned polarizations,[7,23] allowing us to verify the co-aligned nature of the polarization of individual interfaces.

To rationalize these results, we performed DFT calculations of the *r*-MoS$_2$ multilayers (see Section S2.1, Supporting Information), based on the generalized-gradient approximation functional of Perdew, Burke, and Ernzerhof (PBE).[24] As shown in Section 2.1 (Supporting Information), we find that atomic relaxation upon stacking is minute, with minor effect on the calculated polarization. This proves that the mechanism underlying polarization saturation is electronic rather than structural. Importantly, the DFT- computed results, shown as blue upright triangles in Figure 2a, are in qualitative agreement with the experimental results (shown as black symbols for the four devices studied), i.e., showing an initial linear polarization increase with stack thickness followed by polarization saturation. However, quantitative agreement is lacking. The calculated potential saturation value for undoped *r*-MoS$_2$ is roughly twice as large as its experimental counterpart and is obtained at a higher stack thickness of 14 layers, where the potential drop across the stack approaches the PBE-calculated bandgap (≈0.9 V) of bulk *r*-MoS$_2$ under periodic boundary conditions. Importantly, the PBE bandgap seriously underestimates the experimental one, ≈1.3 eV,[25] which is a well-known systematic issue.[26] It has been previously pointed out[27–29] that if the computed bandgap is too small, the critical potential drop at which charge must transfer from the top of the valence band on one surface to the bottom of the conduction band on the other surface, will be reached at a smaller thickness compared to the experimental one. As explained above, it is this charge transfer that causes the saturation of the polarization. Therefore, the computed polarization will saturate prematurely and an underestimated saturated polarization value will follow. Here, however, the exact opposite is found, namely the theoretical values overestimate the experimental ones. Therefore, the discrepancy cannot be attributed to our choice of approximate density functional.

The quantitative discrepancy between experiment and computation can be resolved by considering the effect of free charge carriers in the grown crystals. To examine this, we introduced free electrons in the stacked layers by means of the pseudo-atom approach (see Section S2.1, Supporting Information),[30] which we have previously employed successfully in studies of gated stacked layers.[7] The results obtained in this case are shown as blue downward facing triangles in Figure 2a. Clearly, by introducing a free charge carrier level of 7.5×10^{11} e cm^{-2} per layer, quantitative agreement between theory and experiment (for three of the four devices, with Device 2 likely having a lower effective doping level) is obtained. This free carrier level should be considered as a lower bound of the actual carrier level, as it must also compensate for the above-discussed effect of the gap underestimation. To further verify this idea, we performed self-consistent Poisson–Schrödinger (P–S) calculations that simulate the surface potential variation with increasing layer number under extrinsic charge doping (see Section S3, Supporting Information). The results obtained from these calculations, also shown in Figure 2a, agree well with the DFT calculated polarization curves at both zero doping and at the above-determined free doping level, thereby further confirming our conclusions.

To obtain further insight into the mechanism of polarization saturation, **Figure 3a** presents the electronic density of states (DOS) of a 15-layered *r*-MoS$_2$ stack, projected on individual layers. The DOS corresponding to each layer (colored graphs in the figure) is essentially the same as that of the periodic bulk system (gray graph), except for polarization-induced band shifts that, for a thick enough layer, lead to full bandgap closure, i.e., the valence band maximum on the right edge of the stack is at the same energy as the conduction band minimum at its left edge (see further elaboration in Section S2.2, Supporting Information). The same effect is seen by plotting the band structure (Figure 3b), where each bulk band is expanded into a manifold of bands arising from individual layers, with the VBM and CBM charge densities shown in Figure 3c exhibiting surface charge

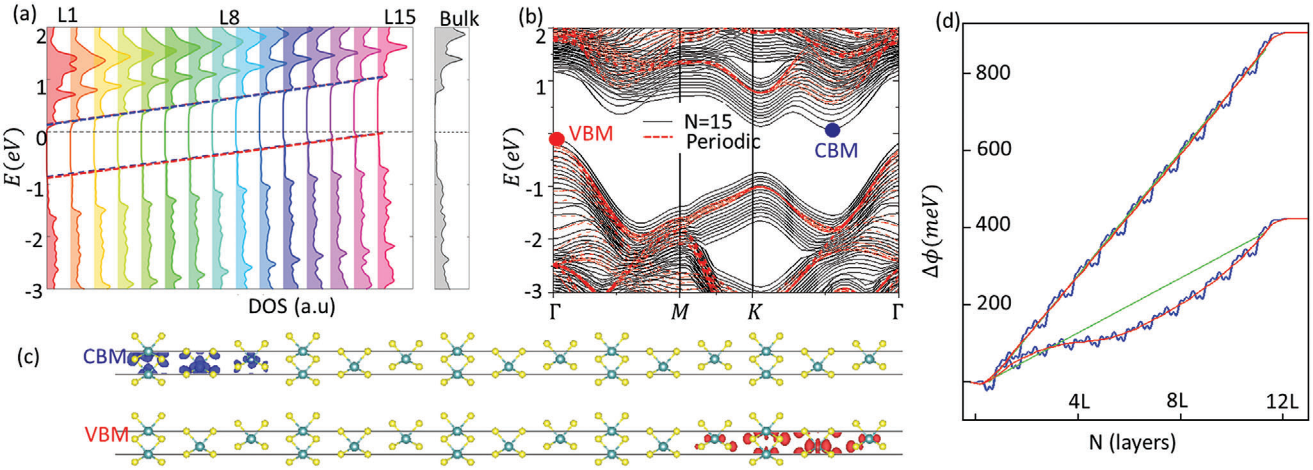

Figure 3. Demonstration of the electronic mechanism for polarization saturation. a) Layer-projected DFT-calculated density of states (DOS) for a 15-layered r-MoS$_2$ stack (color graphs). The red and blue dashed lines denote the varying position of the local valence band maximum (VBM) and conduction band minimum (CBM) across the stack. The dashed-dotted horizontal gray line indicates the Fermi energy. The bulk DOS is given by the gray graph. b) Electronic band structure of the same system (black lines) compared to its bulk counterpart (red lines). The energy origin is chosen as the VBM, with both VBM and CBM positions marked explicitly. c) Charge densities corresponding to the VBM and CBM orbitals of the stack, with an isosurface of 4.8×10^{-6} e Å^{-3}. d) Laterally averaged potential (blue lines) obtained via DFT calculations for an undoped and doped (charge carrier density of 7.5×10^{11} e cm^{-2}) 12-layer r-MoS$_2$ stack. The red line denotes the macroscopic potential, obtained from the laterally averaged one after further perpendicular running-window averaging with a window width of 0.6 nm. The dashed green line demonstrates a linear potential drop. It is virtually indistinguishable from the red line for the undoped case but emphasizes a parabolic behavior of the red line upon doping. All potentials are presented after subtracting the sum of potential profiles of the corresponding individual monolayers.

characteristics. Once the VBM and CBM achieve the same energy, charge transfer occurs between the two outer layers (see Figure 3c and Section S2.3, Supporting Information), inducing an electric field that opposes the polarization.[15] Upon further increase in the layer thickness, the polarization saturates because the potential drop is pinned by the position of the VBM and CBM. Interestingly, in the case of pristine crystals, this charge transfer mechanism, beyond a critical thickness, is expected to produce mobile electron-like states on one surface and hole-like carriers on the other surface.[31–33] A rough estimate for the position of the "knee" is where the shift in DOS owing to the polarization closes the gap. This can be found by equating the overall potential drop prior to saturation, $N{\bullet}V_I$ (where N is the number of layers and V_I is the potential drop associated with a single interface) with the bandgap, E_g. Rounding to the nearest integer, the critical number of stack layers is then $N_c = \mathrm{int}(E_g/V_I) + 1$ (see Section S2.4, Supporting Information, for specific examples). We note that in both experiment and simulations a continuous potential saturation, rather than a sharp "knee," is observed. This is due to the finite electronic temperature and the finite density of states at the band edge.

The role of doping in the polarization saturation is further clarified by plotting the potential drop across the stack with and without doping, for the case of $N = 12$ (see Figure 3d). The figure shows both the laterally averaged local potential (blue line) and the macroscopically averaged potential (red line), obtained from the local one by further averaging within a moving window in the direction perpendicular to the stack, with the window width being 0.6 nm, which is the Mo—Mo distance in adjacent layers. Clearly, for the undoped stack the macroscopic potential drop beyond the immediate surface region is essentially linear with position, as expected for an insulator. For the doped case, however, there is a roughly parabolic deviation from the linear drop, which is the hallmark of the emergence of a space charge region with free carriers.[34] These carriers screen the potential drop, thereby both reducing its final magnitude and promoting the onset of saturation.

The polarization saturation phenomenon, demonstrated here for MoS$_2$ stacks, is of general nature and should be observed for other ladder ferroelectric architectures. Unfortunately, at present 3R crystals of sufficient quality are only available for MoS$_2$, but the effect can still be identified computationally. Figure 2b compares the DFT-calculated polarization curves for undoped r-MoS$_2$, r-WSe$_2$, and r-BN, demonstrating that all three-layered materials exhibit polarization saturation behavior. r-BN exhibits a considerably higher saturation polarization (potential drop of ≈4.5 V) and a larger saturation thickness, $N \approx 40$, owing to its much larger bandgap (see Sections S2.4–S2.5, Supporting Information). Similar correlation between gap closure and polarization saturation is found also for 1T′-ReS$_2$ (see Section S2.6, Supporting Information), which was experimentally shown to exhibit ferroelectric behavior.[35] These findings validate the mechanism proposed in ref. [15] and agree with similar observations for monolayers of polar oligomers.[28,29] Notably, bandgap closure is not observed for nonpolar, antiparallelly stacked AA′ and Bernal AB stacked multilayers, where the gap converges toward its bulk limit with increasing stack thickness (see Section S2.5, Supporting Information). Furthermore, polarization build-up is not observed in semimetallic stacks, e.g., 1T′ WTe$_2$ and MoTe$_2$ (see Section S2.6, Supporting Information), both of which are reported to exhibit interfacial ferroelectricity.[2,36]

3. Conclusion

In conclusion, we have demonstrated experimentally the emergence of polarization saturation in stacked layers of MoS_2. The underlying mechanism, exposed via DFT calculations, agrees with the Ghosez–Gonze–Godby[15] suggestion of polarization-induced bandgap reduction with increasing stack thickness, up to a critical point where bandgap closure facilitates charge transfer that suppresses further polarization increase. However, it goes beyond it by showing that doping provides additional screening that reduces the saturated polarization value and stack thickness at which it is attained. This, along with the newly discovered slidetronic switching mechanism, offers new opportunities for the control and design of polarization in novel electronic components.

Supporting Information

Supporting Information is available from the Wiley Online Library or from the author.

Acknowledgements

W.C., S.D., and M.V.S. contributed equally to this work. O.H. is grateful for the generous financial support of the Ministry of Science and Technology of Israel (Project No. 3-16244) and the Heineman Chair in Physical Chemistry. M.B.S. acknowledges funding by the European Research Council under the European Union's Horizon 2020 research and innovation programme (Grant Agreement No. 852925), and the Israel Science Foundation under Grant Nos. 319/22 and 3623/21. O.H., M.U., and M.B.S. acknowledge the Centre for Nanoscience and Nanotechnology of Tel Aviv University. L.K. thanks the Aryeh and Mintzi Katzman Professorial Chair and the Helen and Martin Kimmel Award for Innovative Investigation.

Conflict of Interest

The authors declare no conflict of interest.

Data Availability Statement

The data that support the findings of this study are available from the corresponding author upon reasonable request.

Keywords

layered van der Waals structures, MoS_2, polarization, slidetronics, transition metal dichalcogenides

Received: January 15, 2024
Revised: April 10, 2024
Published online: May 3, 2024

---

[1] L. Li, M. Wu, *ACS Nano* **2017**, *11*, 6382.
[2] Z. Fei, W. Zhao, T. A. Palomaki, B. Sun, M. K. Miller, Z. Zhao, J. Yan, X. Xu, D. H. Cobden, *Nature* **2018**, *560*, 336.
[3] M. V. Stern, Y. Waschitz, W. Cao, I. Nevo, K. Watanabe, T. Taniguchi, E. Sela, M. Urbakh, O. Hod, M. Ben Shalom, *Science* **2021**, *372*, 1462.
[4] K. Yasuda, X. Wang, K. Watanabe, T. Taniguchi, P. Jarillo-Herrero, *Science* **2021**, *372*, 1458.
[5] C. R. Woods, P. Ares, H. Nevison-Andrews, M. J. Holwill, R. Fabregas, F. Guinea, A. K. Geim, K. S. Novoselov, N. R. Walet, L. Fumagalli, *Nat. Commun.* **2021**, *12*, 347.
[6] X. Wang, K. Yasuda, Y. Zhang, S. Liu, K. Watanabe, T. Taniguchi, J. Hone, L. Fu, P. Jarillo-Herrero, *Nat. Nanotechnol.* **2022**, *17*, 367.
[7] S. Deb, W. Cao, N. Raab, K. Watanabe, T. Taniguchi, M. Goldstein, L. Kronik, M. Urbakh, O. Hod, M. Ben Shalom, *Nature* **2022**, *612*, 465.
[8] P. Meng, Y. Wu, R. Bian, E. Pan, B. Dong, X. Zhao, J. Chen, L. Wu, Y. Sun, Q. Fu, Q. Liu, D. Shi, Q. Zhang, Y.-W. Zhang, Z. Liu, F. Liu, *Nat. Commun.* **2022**, *13*, 7696.
[9] D. Yang, J. Wu, B. T. Zhou, J. Liang, T. Ideue, T. Siu, K. M. Awan, K. Watanabe, T. Taniguchi, Y. Iwasa, M. Franz, Z. Ye, *Nat. Photonics* **2022**, *16*, 469.
[10] S. Zhang, Y. Liu, Z. Sun, X. Chen, B. Li, S. L. Moore, S. Liu, Z. Wang, S. E. Rossi, R. Jing, J. Fonseca, B. Yang, Y. Shao, C.-Y. Huang, T. Handa, L. Xiong, M. Fu, T.-C. Pan, D. Halbertal, X. Xu, W. Zheng, P. J. Schuck, A. N. Pasupathy, C. R. Dean, X. Zhu, D. H. Cobden, X. Xu, M. Liu, M. M. Fogler, J. C. Hone, et al., *Nat. Commun.* **2023**, *14*, 6200.
[11] K. Ko, A. Yuk, R. Engelke, S. Carr, J. Kim, D. Park, H. Heo, H.-M. Kim, S.-G. Kim, H. Kim, T. Taniguchi, K. Watanabe, H. Park, E. Kaxiras, S. M. Yang, P. Kim, H. Yoo, *Nat. Mater.* **2023**, *22*, 992.
[12] S. S. Atri, W. Cao, B. Alon, N. Roy, M. Vizner Stern, V. Fal'ko, M. Goldstein, L. Kronik, M. Urbakh, O. Hod, M. Ben Shalom, *Adv. Phys. Research*, https://doi.org/10.1002/apxr.202300095.
[13] A. Garcia-Ruiz, V. Enaldiev, A. McEllistrim, V. I. Fal'ko, *Nano Lett.* **2023**, *23*, 4120.
[14] L. Yang, S. Ding, J. Gao, M. Wu, *Phys. Rev. Lett.* **2023**, *131*, 096801.
[15] X. Gonze, P. Ghosez, R. W. Godby, *Phys. Rev. Lett.* **1997**, *78*, 294.
[16] M. Stutzmann, O. Ambacher, M. Eickhoff, U. Karrer, A. Lima Pimenta, R. Neuberger, J. Schalwig, R. Dimitrov, P. J. Schuck, R. D. Grober, *Phys. Status Solidi B* **2001**, *228*, 505.
[17] N. Nakagawa, H. Y. Hwang, D. A. Muller, *Nat. Mater.* **2006**, *5*, 204.
[18] P. R. Willmott, S. A. Pauli, R. Herger, C. M. Schlepütz, D. Martoccia, B. D. Patterson, B. Delley, R. Clarke, D. Kumah, C. Cionca, Y. Yacoby, *Phys. Rev. Lett.* **2007**, *99*, 155502.
[19] J. Lähnemann, O. Brandt, U. Jahn, C. Pfüller, C. Roder, P. Dogan, F. Grosse, A. Belabbes, F. Bechstedt, A. Trampert, L. Geelhaar, *Phys. Rev. B* **2012**, *86*, 081302.
[20] B. S. Eller, J. Yang, R. J. Nemanich, *J. Vac. Sci. Technol. A* **2013**, *31*, 050807.
[21] C. F. Chang, et al., *Phys. Rev. X* **2016**, *6*, 041011.
[22] P. W. Lee, V. N. Singh, G. Y. Guo, H.-J. Liu, J.-C. Lin, Y.-H. Chu, C. H. Chen, M.-W. Chu, *Nat. Commun.* **2016**, *7*, 12773.
[23] J. Liang, D. Yang, Y. Xiao, S. Chen, J. I. Dadap, J. Rottler, Z. Ye, *Nano Lett.* **2023**, *23*, 7228.
[24] J. P. Perdew, K. Burke, M. Ernzerhof, *Phys. Rev. Lett.* **1996**, *77*, 3865.
[25] K. F. Mak, C. Lee, J. Hone, J. Shan, T. F. Heinz, *Phys. Rev. Lett.* **2010**, *105*, 136805.
[26] S. Kümmel, L. Kronik, *Rev. Mod. Phys.* **2008**, *80*, 3.
[27] E. Rudberg, *J. Phys.: Condens. Matter* **2012**, *24*, 072202.
[28] F. Rissner, A. Natan, D. A. Egger, O. T. Hofmann, L. Kronik, E. Zojer, *Org. Electron.* **2012**, *13*, 3165.
[29] G. Lever, D. J. Cole, N. D. M. Hine, P. D. Haynes, M. C. Payne, *J. Phys.: Condens. Matter* **2013**, *25*, 152101.
[30] O. Sinai, L. Kronik, *Phys. Rev. B* **2013**, *87*, 235305.
[31] A. Ohtomo, H. Y. Hwang, *Nature* **2004**, *427*, 423.
[32] F. Brivio, A. M. Rappe, L. Kronik, D. Ritter, *Appl. Phys. Lett.* **2023**, *123*, 022104.
[33] S.-H. Yoo, M. Todorova, J. Neugebauer, C. G. Van de Walle, *Phys. Rev. Appl.* **2023**, *19*, 064037.
[34] A. Many, Y. Goldstein, N. B. Grover, *Semiconductor Surfaces*, North-Holland, Amsterdam **1965**.

[35] Y. Wan, T. Hu, X. Mao, J. Fu, K. Yuan, Y. Song, X. Gan, X. Xu, M. Xue, X. Cheng, C. Huang, J. Yang, L. Dai, H. Zeng, E. Kan, *Phys. Rev. Lett.* **2022**, *128*, 067601.

[36] A. Jindal, A. Saha, Z. Li, T. Taniguchi, K. Watanabe, J. C. Hone, T. Birol, R. M. Fernandes, C. R. Dean, A. N. Pasupathy, D. A. Rhodes, *Nature* **2023**, *613*, 48.